Journal of Nanofluids
Vol. 11, pp. 31–38, 2022
(www.aspbs.com/jon)

Heat Transfer on Magnetohydrodynamics Squeezing Flow of Jeffrey Fluid Through Permeable Medium with Slip Boundary

Nur Azlina Mat Noor, Sharidan Shafie, and Mohd Ariff Admon*

Department of Mathematical Sciences, Faculty of Science, Universiti Teknologi Malaysia, Johor Bahru, 81310, Johor, Malaysia

The hydromagnetic squeeze flow and heat transfer of Jeffrey fluid in two plates over permeable medium is investigated. The effects of slip condition and viscous dissipation are considered in the mathematical model. Transformation of the partial differential equations (PDEs) to ordinary differential equations (ODEs) is performed by imposing similarity variables. Numerical procedure of Keller-box is employed to solve the dimensionless equations. The solutions for skin friction are compared with published solutions from the journal to validate the current solutions and it is shown in close agreement. The physical behavior of velocity and wall shear stress are analyzed for squeezing parameter. The results show the acceleration of wall shear stress and velocity when the surfaces approaching each other. The increment of Jeffrey fluid and Hartmann parameters decrease the velocity and temperature. The temperature and the rate of thermal transfer boosts with the existence of viscous dissipation.

KEYWORDS: Jeffrey Fluid, Squeeze Flow, Magnetohydrodynamic, Porous Medium, Slip Condition.

1. INTRODUCTION

Squeeze flow is produced by imposing the external stress on the plates towards each other. The flow has obtained great interest from scientists as the concept of squeeze flow is useful in engineering applications involving model of oil flow in the bearings, lubrication systems, injection molding and hydraulic lifts.[1] The fundamental research on mathematical model of viscous fluid in the two moving plates using lubrication system was introduced by Stefan.[2] Following pioneer work of Stefan, many researchers have carried out various research attempts on squeeze flow with various configurations and boundary conditions.[3–8]

Jeffrey fluid is one of simpler model of non-Newtonian fluid that exhibit both viscosity and elasticity properties. It is categorized as shear thinning fluid due to the presence of yield stress and high shear viscosity. It acts similar as Newtonian fluid when the shear stress applied is greater than yield stress.[9] The relaxation and retardation times in Jeffrey fluid model is substantial to represent the viscoelastic features in the polymer materials.[10] Sharma et al.[11] reported that Jeffrey fluid is used for mathematical model of blood flow through narrow arteries. It is also implemented in biological system of fluid transport, which known as peristalsis.[12, 13]

The study of flow through porous medium has been a growing research interest because of the current improvement in the Darcy Law formula. It is found in natural and industrial problems, especially in geophysical fluid dynamics such as geothermal energy recovery, plasma studies, oil extraction and nuclear reactors.[14–16] Furthermore, the research on flow of magnetohydrodynamics (MHD) is important in the application of electromagnetic pump. The pumping motion is generated mechanically by Lorentz force.[17–19] Several researchers have reviewed the flow of Jeffrey fluid in various flow configurations. Hayat et al.[20] analyzed the presence of suction and injection on MHD squeeze flow of Jeffrey fluid in a permeable channel via analytical approach of homotopy analysis method (HAM). Muhammad et al.[21] continued Hayat et al.[20] work with MHD flow across stretching lower plate. Further, Ahmad and Ishak[22] explored the mixed convection flow of Jeffrey fluid near a stagnation point. The movement of flow is due to the stretched vertical sheet under the impact of magnetic field. The problem was solved by imposing Keller-box approach.

The above-mentioned literature discovers that the study on squeeze flow of Jeffrey fluid with magnetic field is limited. Moreover, there is no study considering slip boundary condition. Motivated by the cited papers, the present

*Author to whom correspondence should be addressed.
Email: ariffadmon@utm.my
Received: 23 May 2021
Accepted: 15 July 2021

ARTICLE

research investigates the heat transfer on unsteady MHD squeezing flow of Jeffrey fluid in two surfaces across permeable medium. The velocity slip is taken into account at the upper surface. The resulting equations are computed via Keller-box technique. The present results are validated through comparison with existing literature results and revealed in close agreement. The behaviour of velocity and temperature profile is examined graphically.

2. MATHEMATICAL FORMULATION

The time dependent MHD flow of Jeffrey fluid through porous medium with slip velocity is considered. The squeezing of two surfaces generates the flow in the channel. The distance of two surfaces is $y = \pm h(t) = \pm l(1-\alpha t)^{1/2}$. The two surfaces are moving further as $\alpha < 0$ and the surfaces are moving closer as $\alpha > 0$ till $t = 1/\alpha$ with velocity $v_w(t) = (\partial h(t)/\partial t)$. The lower plate is exerted with the magnetic field $B(t)$ vertically. Figure 1 illustrates the geometrical model of Jeffrey fluid flow.

The governing equations of Jeffrey fluid are reduced to the following equations using boundary layer approximation[23]

$$\frac{\partial u}{\partial x}+\frac{\partial v}{\partial y}=0 \tag{1}$$

$$\begin{aligned}&\frac{\partial u}{\partial t}+u\frac{\partial u}{\partial x}+v\frac{\partial u}{\partial y}\\&=\nu_f\left(1+\frac{1}{\lambda_1}\right)\frac{\partial^2 u}{\partial y^2}+\nu_f\frac{\lambda_2}{1+\lambda_1}\\&\times\left(\begin{array}{l}\dfrac{\partial^3 u}{\partial t\partial y^2}+u\dfrac{\partial^3 u}{\partial x\partial y^2}\\+v\dfrac{\partial^3 u}{\partial y^3}-\dfrac{\partial u}{\partial x}\dfrac{\partial^2 u}{\partial y^2}+\dfrac{\partial u}{\partial y}\dfrac{\partial^2 u}{\partial x\partial y}\end{array}\right)\\&-\frac{\sigma B^2(t)}{\rho_f}u-\nu_f\left(1+\frac{1}{\lambda_1}\right)\frac{\phi}{k_1(t)}u\end{aligned} \tag{2}$$

$$\begin{aligned}&\frac{\partial T}{\partial t}+u\frac{\partial T}{\partial x}+v\frac{\partial T}{\partial y}\\&=\alpha_f\frac{\partial^2 T}{\partial y^2}+\frac{\nu_f}{c_f}\left(1+\frac{1}{\beta}\right)\\&\times\left[4\left(\frac{\partial u}{\partial x}\right)^2+\left(\frac{\partial u}{\partial y}\right)^2\right]\end{aligned} \tag{3}$$

Here, the thermal diffusion of Jeffrey fluid is $\alpha_f = (k/(\rho c)_f)$ and the permeability of porous medium is $k_1(t) = k_0(1-\alpha t)$.

The correlated boundary conditions (BCs) are[24]

$$\begin{gathered}u=N_1\nu_f\left(1+\frac{1}{\lambda_1}\right)\frac{\partial u}{\partial y},\quad v=v_w=\frac{\partial h(t)}{\partial t},\\T=T_w,\quad\text{at}\quad y=h(t)\end{gathered} \tag{4}$$

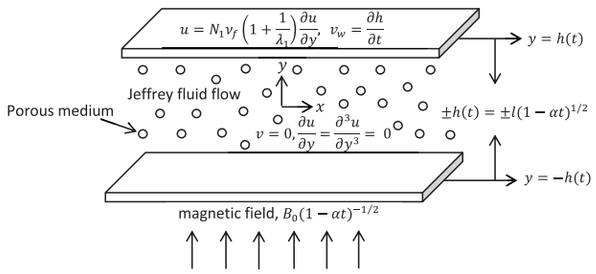

Fig. 1. Geometrical model.

$$\frac{\partial u}{\partial y}=0,\quad \frac{\partial^3 u}{\partial y^3}=0,\quad v=0,\quad \frac{\partial T}{\partial y}=0,\quad\text{at}\quad y=0 \tag{5}$$

where $N_1(t) = N_0(1-\alpha t)^{1/2}$ represent momentum slip.

The similarity transformation applied in Usman et al.[25] is imposed to transform the PDEs into dimensionless ODEs;

$$\begin{gathered}u=\frac{\alpha x}{2(1-\alpha t)}f'(\eta),\quad v=-\frac{\alpha l}{2\sqrt{(1-\alpha t)}}f(\eta),\\\eta=\frac{y}{l\sqrt{(1-\alpha t)}},\quad \theta=\frac{T}{T_w}\end{gathered} \tag{6}$$

Substitute Eq. (7) into Eqs. (2)–(4) yields to obtain the subsequent non dimensional equations.

$$\begin{aligned}&\left(1+\frac{1}{\lambda_1}\right)f^{iv}-S(\eta f'''+3f''+f'f''-ff''')\\&+\left(1+\frac{1}{\lambda_1}\right)\frac{De}{2}(\eta f^v+5f^{iv}+2f''f'''-f'f^{iv}-ff^v)\\&-Ha^2f''-\left(1+\frac{1}{\lambda_1}\right)\frac{1}{Da}f''=0\end{aligned} \tag{7}$$

$$\begin{aligned}&\frac{1}{Pr}\theta'+S(f\theta'-\eta\theta')\\&+Ec\left[\left(1+\frac{1}{\beta}\right)[(f'')^2+4\delta^2(f')^2]\right]=0\end{aligned} \tag{8}$$

with the non-dimensional BCs

$$\begin{gathered}f(\eta)=0,\quad f''(\eta)=0,\quad f^{iv}(\eta)=0,\\\theta'(\eta)=0,\quad\text{at}\quad\eta=0\end{gathered} \tag{9}$$

$$\begin{gathered}f(\eta)=1,\quad f'(\eta)=\gamma\left(1+\frac{1}{\lambda_1}\right)f''(\eta),\\\theta(\eta)=1,\quad\text{at}\quad\eta=1\end{gathered} \tag{10}$$

The pertinent terms in the non-dimensional equations are described by

$$\begin{gathered}S=\frac{\alpha l^2}{2\nu_f},\quad Ha=lB_0\sqrt{\frac{\sigma}{\rho_f\nu_f}},\quad Da=\frac{k_0}{\phi l^2},\\De=\frac{\alpha\lambda_2}{1-\alpha t},\quad \gamma=\frac{N_0\nu_f}{l},\quad \delta=\frac{l}{x}(1-\alpha t)^{1/2},\\Ec=\frac{\alpha^2x^2}{4c_f(T_w-T_\infty)(1-\alpha t)^2},\quad Pr=\frac{\nu_f}{\alpha_f}\end{gathered} \tag{11}$$

3. RESULTS AND DISCUSSION

The governing nonlinear ODEs (7)–(8) with BCs (9) and (10) is resolved via Keller-box procedure. MATLAB software is employed to obtain the graphical and numerical outputs. Proper values of the step size, $\Delta\eta = 0.01$ and boundary layer thickness, $\eta_\infty = 1$ are chosen to obtain the accurate solutions. The variation in the current and former results of concentration, temperature and velocity is described as convergence criterion. Calculation is ended when the numerical outputs converging to 10^{-5}.[26] The four steps in the Keller box scheme are:

(i) Convert the ODEs into a system of first order equations.

(ii) The first order equations are discretized by implementing the central difference approach.

(iii) Apply Newton's method for linearization the governing equations.

(iv) The linear system is solved via block tri-diagonal elimination approach.

The numerical calculations for various parameters S, λ_1, Ha, Da, De, γ, Ec and Pr are done to explore the behaviour of velocity and temperature profile graphically. The skin friction for different S values is compared with Wang,[4] Khan et al.[7] and Naduvinamani and Shankar[27] as limiting cases and depicted in Table I. The proper agreement is observed from the outputs.

The effects of S on velocity and temperature profiles are analysed in Figures 2–4. The movement of surfaces approaching closer is described by $S > 0$ and the movement of surfaces separating apart is described by $S < 0$. Figure 2 depicts the velocity decreasing as $S > 0$, meanwhile the velocity increasing as $S < 0$ in the boundary layer. The fluid inside the channel is pushed out caused by squeezing of surfaces, which resulting in decelerating the velocity field. Meanwhile, the increment of velocity owing to the fluid is pushed into the channel as the surfaces separates further. The impact of S on axial velocity is portrayed in Figure 3. It is noted that the area close to the lower surface is $0 \leq \eta < 0.45$ and the area close to the upper surface is $0.45 \leq \eta \leq 1$. For $S > 0$, the velocity slows down as $\eta < 0.45$ and it elevates as $\eta \geq 0.45$. For $S < 0$, the

Table I. Numerical results of $-f''(1)$ for S when $\lambda_1 \to \infty$, $Da \to \infty$, $Ha = \gamma = 0$ and $De = 10^{-10}$.

	$-f''(1)$			
S	Wang[4]	Khan et al.[7]	Naduvinamani and Shankar[27]	Present results
−0.9780	2.235	2.1915	2.1915	2.1917
−0.4977	2.6272	2.6193	2.6193	2.6194
−0.09998	2.9279	2.9277	2.9277	2.9277
0	3.000	3.000	3.000	3.000
0.09403	3.0665	3.0663	3.0663	3.0664
0.4341	3.2969	3.2943	3.2943	3.2943
1.1224	3.714	3.708	3.708	3.708

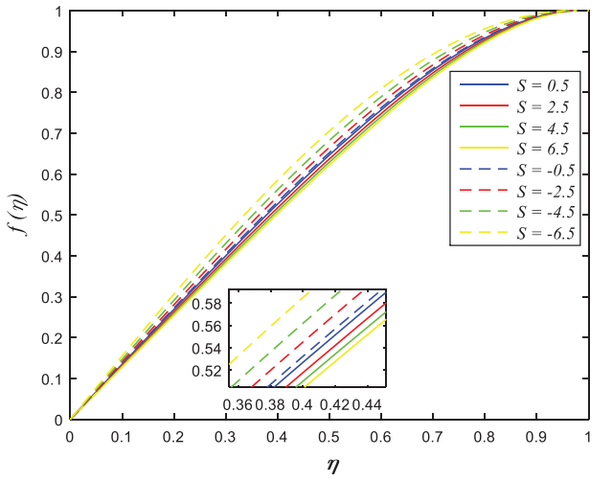

Fig. 2. Influence of S on $f(\eta)$.

velocity rises as $\eta < 0.45$ and it reduces as $\eta \geq 0.45$. The fluid across the narrow channel rapidly when the surfaces approaching one another and consequently, enhances the velocity nearby the upper surface area. On the contrary, the velocity drops due to the flow encounter more resistancy in the wider channel. The cross-behavior of fluid flow arises at the midpoint of boundary section. At the critical point $\eta_c = 0.45$, no significant effect on the velocity is discovered when varying squeeze values. The effects of S on temperature field is displayed in Figure 4. The temperature decreasing for $S > 0$ and it enhances for $S < 0$. When the surfaces approach closer, the kinetic energy in fluid particles decelerates and thus, reduces the temperature of the flow. The movement of plates did not vary the temperature adjacent to the upper boundary $\eta = 1$.

The variation of λ_1 on velocity and temperature field are illustrated in Figures 5–7. The radial velocity from Figure 5 declines when λ_1 increasing. The reason is that the intermolecular forcés of fluid particles become

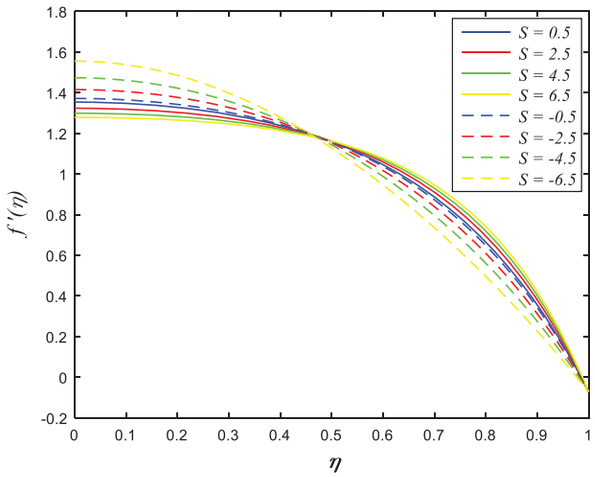

Fig. 3. Influence of S on $f'(\eta)$.

ARTICLE

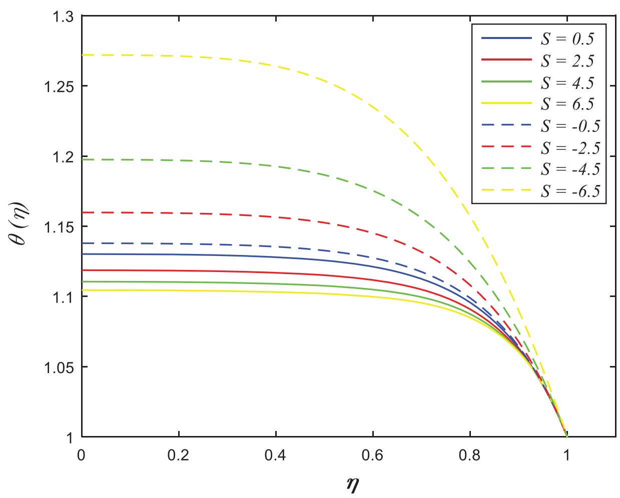

Fig. 4. Influence of S on $\theta(\eta)$.

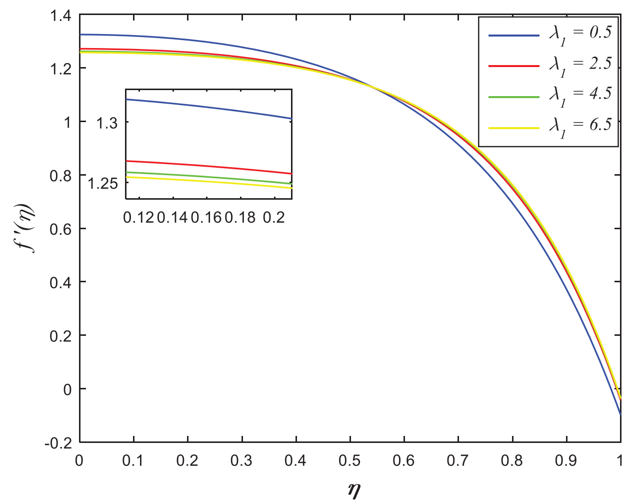

Fig. 6. Influence of λ_1 on $f'(\eta)$.

strenghten caused by the fluid viscosity rises as λ_1 increases. Hence, it has caused the fluid flow slowing down in the channel. Figure 7 presents the axial velocity decreasing as $\eta \leq 0.5$ and it elevates as $\eta > 0.5$ with increment in λ_1. The impact of λ_1 on temperature is demonstrated in Figure 7. The temperature reduces with enhance in λ_1. It is due to fact the higher flow viscosity strengthens the intermolecular forces of fluid particles. Hence, the decrease in kinetic energy lead to the flow temperature declines.

Figures 8 to 10 reveal the variation of Ha on velocity and temperature field. The reduction of normal velocity is noticed from Figure 8 when Ha increases. Physically, the magnetic field in the electrical conducted fluid generates Lorentz force. The presence of this force increases the resistancy that oppose the flow in the channel. Figure 9 shows that for $\eta \leq 0.5$, the axial velocity decelerates and for $\eta > 0.5$, it accelerates for increasing Ha. The influence of Ha on temperature is plotted in Figure 10. It is noted that the temperature dropping for $\eta \leq 0.8$ and it increasing for $\eta > 0.8$ with raise in Ha.

The influence of Da on axial velocity is exhibited in Figure 11. For $\eta \leq 0.5$, the velocity elevating and for $\eta > 0.5$, it drops as Da increasing. The raise in the permeability of porous medium boosts the fluid flow through porous medium at the center of channel. Figure 12 demonstrates the variation of γ on axial velocity. The velocity slip at the upper surface happens if the velocity of the surface and the fluid velocity next to the surface is diverse. For $\eta \leq 0.6$, the velocity enhances and for $\eta > 0.6$, it decreasing when γ rises. The increment of γ implies that more fluid able to slip through the upper surface, which result in the flow near the surface slows down. The effect of De on axial velocity is displayed in Figure 13. The velocity accelerates nearby the lower surface and it declining nearby the upper surface as De rises. The ratio of retardation time to the time of observation is represented by Deborah number. Retardation time is the delayed response to an

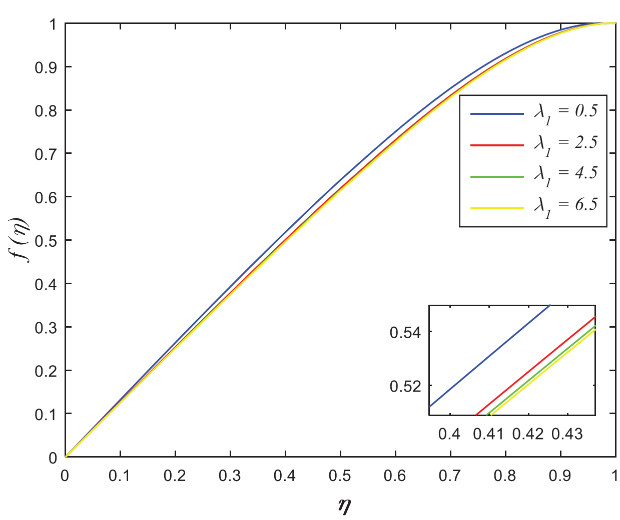

Fig. 5. Influence of λ_1 on $f(\eta)$.

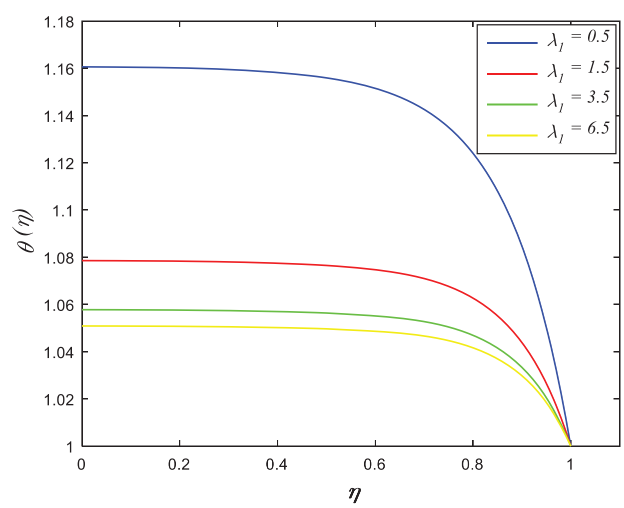

Fig. 7. Effect of λ_1 on temperature.

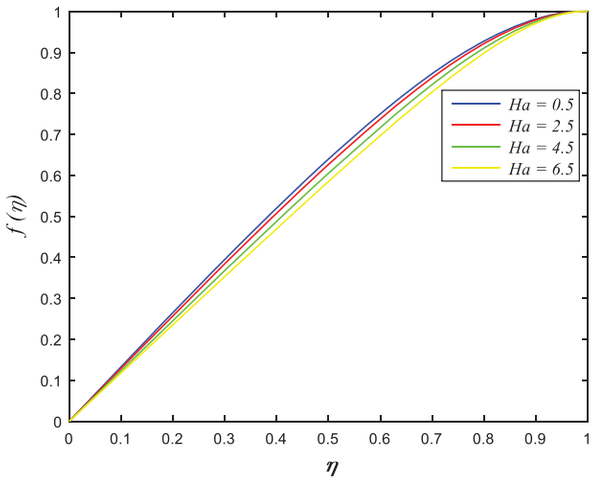

Fig. 8. Influence of Ha on $f(\eta)$.

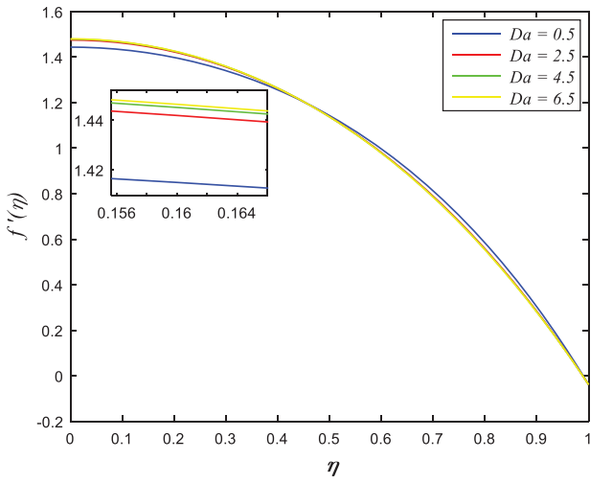

Fig. 11. Influence of Da on $f'(\eta)$.

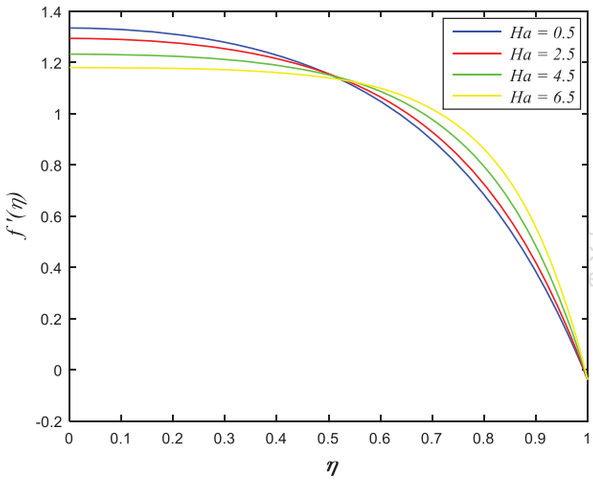

Fig. 9. Influence of Ha on $f'(\eta)$.

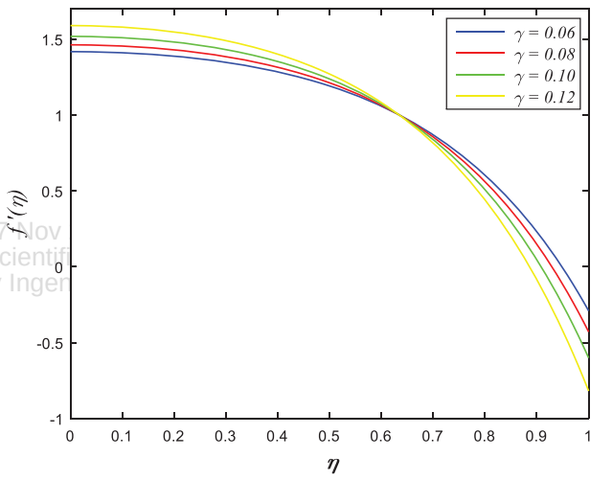

Fig. 12. Influence of γ on $f'(\eta)$.

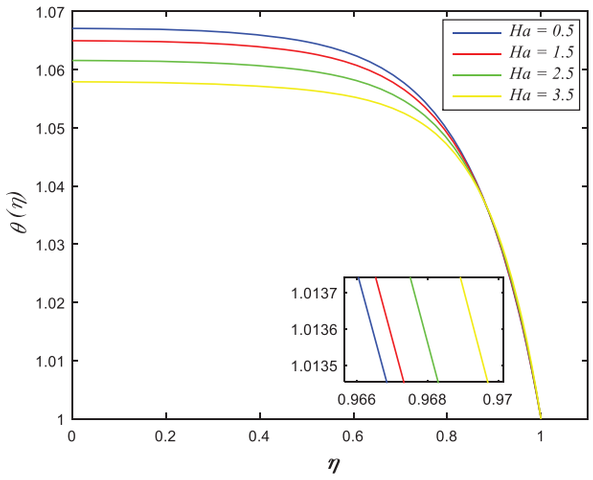

Fig. 10. Effect of Ha on temperature.

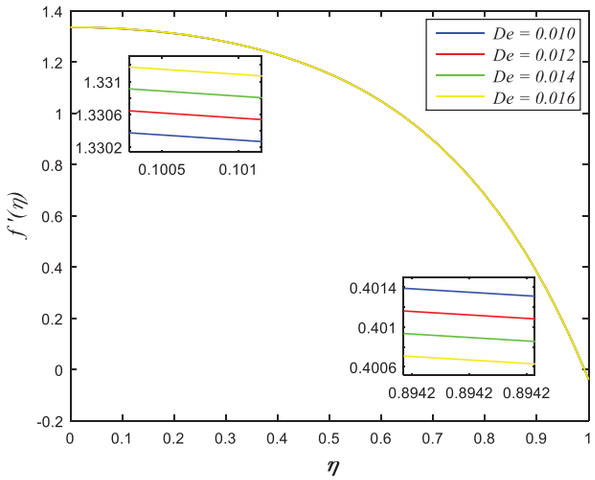

Fig. 13. Influence of De on $f'(\eta)$.

applied stress or 'delay of elasticity.' The fluid has high retardation time for increasing values of De. It shown that the intermolecular forces between fluid particles strengthen because the fluid reacts to the external force slowly. It decelerates the flow next to the upper surface area.

Figure 14 describes the impact of Pr on temperature field. The temperature in the flow elevates as Pr rises. Prandtl number is the ratio of momentum diffusivity to thermal diffusivity. The higher Pr lead to decline in thermal diffusion of Casson fluid and thus, elevates the flow temperature. The influences of Ec on temperature field is presented in Figure 15. It is found that the temperature is shown boosts with enhancement in Ec. The heat induction caused by the friction of fluid particles in the high viscosity flow is called viscous dissipation effect. High values of Ec cause an increment in the kinetic energy. Thus, it raises the friction amongst fluid particles, which resulting in the elevation of the temperature field.

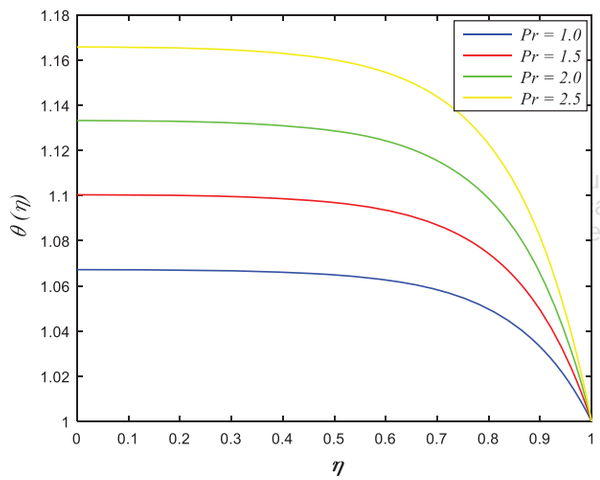

Fig. 14. Influence of Pr on $\theta(\eta)$.

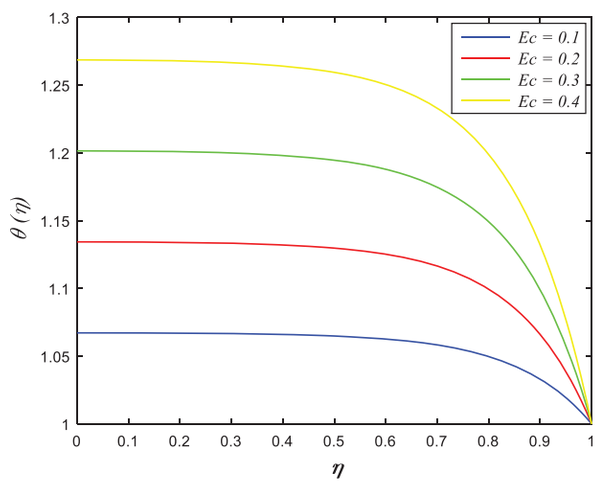

Fig. 15. Influence of Ec on $\theta(\eta)$.

4. PHYSICAL QUANTITY OF INTEREST

Physically, the dimensionless parameters of interest in the fluid are skin friction and Nusselt terms. The friction force at the surface boundary is described by skin friction. Moreover, Nusselt term represent the rate of thermal transfer in the fluid and surfaces. The terms of Cf_x and Nu_x are given as follows[28]

$$Cf_x = \frac{\mu_B\,(1+(1/\lambda_1))\,[(\partial u/\partial y)]_{y=h(t)}}{\rho_f v_w^2},$$

$$Nu_x = \frac{-l\alpha_f(\partial T/\partial y)_{y=h(t)}}{\alpha_f T_w}$$

The non-dimensional of Cf_x and Nu_x are

$$\frac{l^2}{x^2}(1-\alpha t)Re_x Cf_x = (1+(1/\lambda_1))\,f''(1),$$

$$\sqrt{(1-\alpha t)}Nu_x = -\theta'(1)$$

The numerical outputs of skin friction and Nusselt parameters are demonstrated in Table II. The wall shear

Table II. Numerical results of $-(1+1/\lambda_1)f''(1)$ for S, λ_1, Ha, Da, γ and De.

S	λ_1	Ha	Da	γ	De	$-(1+1/\lambda_1)f''(1)$
−1.5	1.5	0.1	1	0.01	0.01	4.444929
−1.0						4.866867
−0.5						5.253721
0						5.611752
0.5						5.945698
1.0						6.259225
1.5						6.555223
1.0	1.0	0.1	1	0.01	0.01	7.465567
	1.5					6.259225
	2.0					5.664561
	2.5					5.310315
	3.0					5.075164
	3.5					4.907676
1.0	1.5	1.0	1.0	0.01	0.01	6.430432
		1.5				6.640604
		2.0				6.924462
		2.5				7.273334
		3.0				7.678004
		3.5				8.129483
1.0	1.5	0.1	1.0	0.01	0.01	6.259225
			1.5			6.161199
			2.0			6.111640
			2.5			6.081726
			3.0			6.061708
			3.5			6.047372
1.0	1.5	0.1	1.0	0.01	0.01	6.259225
				0.03		6.985274
				0.05		7.901797
				0.07		9.095371
				0.09		10.882458
1.0	1.5	0.1	1.0	0.01	0.010	6.259225
					0.011	6.258774
					0.012	6.258324
					0.013	6.257874
					0.014	6.257479

Table III. Numerical results of $-\theta'(1)$ for Pr and Ec when $\gamma = De = 0.01$, $Ha = \delta = 0.1$, $S = Da = 1$ and $\lambda_1 = Sc = R = 1.5$.

Pr	Ec	$-\theta'(1)$
1.0	0.1	0.557395
1.5		0.827020
2.0		1.090918
2.5		1.349315
3.0		1.602427
1.5	0.1	0.827020
	0.2	1.654041
	0.3	2.481061
	0.4	3.308081
	0.5	4.135101
	0.6	4.962122

stress elevates with enhance in S, Ha and γ, meanwhile it decreases for enhancing λ_1, Da and De. The squeezing of surfaces raise the flow in the channel and consequently, enhances the friction force within the fluid and the solid boundary. The existence of Lorentz force and velocity slip cause the wall shear stress accelerates. In contrast, the deceleration of the wall shear stress is due to high values of λ_1 and De boost the intermolecular force of fluid particles. It decelerates the velocity in the boundary region. Besides, the flow via permeable medium encounter a drag force, which result in the flow decreases. Therefore, the drop in the velocity cause the wall shear stress declines. Table III illustrates the impacts of Pr and Ec on Nusselt number. The enhancement of Pr and Ec boost the rate of thermal transfer. Nusselt number is the ratio of convection thermal transfer to conduction thermal transfer. Higher Pr and Ec values raise the flow temperature, which resulting in the convective thermal transfer increases.

5. CONCLUSION

The unsteady MHD squeezing flow of Jeffrey fluid through permeable medium in the presence of velocity slip and viscous dissipation was explored numerically. The conversion of governing PDEs to ODEs via dimensionless variables is carried out. Numerical results are obtained using Keller box method, and graphical solution are computed by MATLAB software. The impact of S, λ_1, Ha, Da, γ, De, Pr and Ec on velocity and temperature are studied. The important outcomes in the results are deduced as:

(1) The velocity adjacent the upper plate region increasing as the surfaces approach closer ($S > 0$) and it decreasing as the surfaces separate further ($S < 0$).

(2) The wall shear stress elevating as S, Ha and γ rises, meanwhile it declining for enhancing λ_1, Da and De.

(3) The increment of λ_1, Ha, Da, γ and De decelerate the velocity nearby the upper plate area.

(4) The temperature and heat transfer rate boost for increasing Pr and Ec.

The flow problem of present study is applicable to be implemented in modelling water pressured nuclear reactor. It is used in the nuclear power plants for electricity generation. Physically, the electricity induced by nuclear reactor boosts under the impact of magnetic field in the fluid flow. It is discovered that MHD exhibits the highest efficiency of power conversion.[29] The slip condition is considered in the boundary surface of nuclear reactor model for adaptation in the practical industry. It is proposed as the fluid velocity no longer adhere to the velocity of boundary surface.[30] Furthermore, the fluid flow with permeable médium enhances the heat removal in the nuclear reactor. It has caused the thermal hydraulic issues such as high temperature fluctuations because of thermal striping and stratifications decreases.[31, 32]

For future works, it is recommended to further this study by investigating unsteady squeezing flow of Jeffrey nanofluid in the effect of thermal radiation. Many researchers explored that the thermal conductivity of fluid could be enhanced with the presence of nanoparticles. The application of nanofluid as a coolants in thermal based devices is important because it has result in energy saving and emisión reduction.[33, 34]

NOMENCLATURE

B	Magnetic field
De	Deborah number
Da	Darcy number
h	Distance between two surfaces
Ha	Hartmann number
k_1	Permeability of porous medium
l	Initial distance of two surfaces
N_1	Velocity slip
S	Squeeze number
t	Time
v_w	Velocity at upper surface
u	Velocity in x direction
v	Velocity in y direction
(x, y)	Cartesian coordinates

Greek Symbols

α	Constant
δ	Dimensionless length
η	Boundary layer thickness
f	Dimensionless velocity parameter
γ	Slip parameter
ν_f	Kinematic viscosity
ϕ	Porosity of permeable medium
ρ_f	Density of fluid
σ	Electrical conductivity
λ_1	Ratio of relaxation and retardation times
λ_2	Retardation time
ν_f	Kinematic viscosity

Acknowledgment: The author would like to acknowledge Ministry of Education (MOE) and Research

Management Centre of Universiti Teknologi Malaysia (UTM), FRGS/1/2019/STG06/UTM/02/22, 5F278 and 08G33.

References and Notes

1. T. Hayat, T. Muhammad, A. Qayyum, A. Alsaedi, and M. Mustafa, *J. Mol. Liq.* 213, 179 **(2016)**.
2. M. Stefan, *The London, Edinburgh and Dublin Philosophical Magazine and Journal of Science* 47, 465 **(1874)**.
3. R. J. Grimm, *Appl. Sci. Res.* 32, 149 **(1976)**.
4. C. Y. Wang, *Journal of App. Mechanics* 43, 579 **(1976)**.
5. N. M. Bujurke, P. K. Achar, and N. P. Pai, Computer extended series for squeezing flow between plates. *Fluid Dynamics Research* 16, 173 **(1995)**.
6. M. Rashidi, H. Shahmohamadi, and S. Dinarvand, *Mathematical Problems in Engineering* 935095, 1 **(2008)**.
7. U. Khan, N. Ahmed, S. I. Khan, Z. A. Zaidi, Y. Xiao-Jun, and S. T. Mohyud-Din, On unsteady two-dimensional and axisymmetric squeezing flow between parallel plate. *Alexandria Engineering Journal* 53, 463 **(2014)**.
8. N. A. M. Noor, S. Shafie, and M. A. Admon, *Journal of Advanced Research in Fluid Mechanics and Thermal Sciences* 68, 94 **(2020)**.
9. S. A. Gaffar, V. R. Prasad, and O. A. Bég, *Alexandria Engineering Journal* 54, 829 **(2015)**.
10. A. Ali and S. Asghar, *Journal of Aerospace Engineering* 27, 644 **(2012)**.
11. B. D. Sharma, P. K. Yadav, and A. Filippov, *Colloid J.* 79, 849 **(2017)**.
12. M. V. Krishna, K. Bharathi, and A. J. Chamkha, *Interfacial Phenomena and Heat Transfer* 6, 253 **(2018)**.
13. N. A. M. Noor, S. Shafie, and M. A. Admon, *Mathematics* 9, 1215 **(2021)**.
14. M. V. Krishna, *International Communications in Heat and Mass Transfer* 119, 104927 **(2020)**.
15. M. V. Krishna and A. J. Chamkha, *Results in Physics* 15, 102652 **(2019)**.
16. M. V. Krishna, N. A. Ahamad, and A. J. Chamkha, *Alexandria Engineering Journal* 60, 845 **(2021)**.
17. N. A. M. Noor, S. Shafie, and M. A. Admon, *Plos One* 16, e0250402 **(2021)**.
18. M. V. Krishna and A. J. Chamkha, *Journal of Porous Media* 22, 209 **(2019)**.
19. M. V. Krishna and A. J. Chamkha, *International Communications in Heat and Mass Transfer* 113, 104494 **(2020)**.
20. T. Hayat, R. Sajjad, and S. Asghar, *Communications in Nonlinear Science and Numerical Simulation* 15, 2400 **(2010)**.
21. T. Muhammad, T. Hayat, A. Alsaedi, and A. Qayyum, *Chinese Journal of Physics* 55, 1511 **(2017)**.
22. K. Ahmad and A. Ishak, *Thermal Science* 6, 269 **(2017)**.
23. N. A. M. Noor, S. Shafie, and M. A. Admon, *Phys. Scr.* 96, 035216 **(2021)**.
24. N. A. M. Noor, S. Shafie, and M. A. Admon, *Phys. Scr.* 95, 105213 **(2020)**.
25. M. Usman, M. Hamid, U. Khan, S. T. Mohyud-Din, M. A. Iqbal, and W. Wang, *Alexandria Engineering Journal* 57, 1867 **(2017)**.
26. N. A. M. Noor, S. Shafie, and M. A. Admon, *MATEMATIKA* 35, 33 **(2019)**.
27. N. B. Naduvinamani and U. Shankar, *Sadhana* 44, 175 **(2019)**.
28. N. A. M. Noor, S. Shafie, and M. A. Admon, *The European Physical Journal Plus* 135, 1 **(2019)**.
29. J. Song, W. An, Y. Wu, and W. Tian, *Frontiers in Energy Research* 6, 1 **(2018)**.
30. H. Saadati, K. Hadad, and A. Rabiee, *Nuclear Engineering and Technology* 50, 639 **(2018)**.
31. P. B. A. Reddy, S. Suneetha, and N. B. Reddy, *Propulsion and Power Research* 6, 259 **(2017)**.
32. A. S. Dogonchi, T. Tayebi, N. Karimi, A. J. Chamkha, and H. Alhumade, *Journal of the Taiwan Institute of Chemical Engineers* 124, 162 **(2021)**.
33. Y. Menni, A. J. Chamkha, and A. Azzi, *J. Nanofluids* 8, 893 **(2019)**.
34. M. S. Sadeghi, A. S. Dogonchi, M. Ghodrat, A. J. Chamkha, H. Alhumade, and N. Karimi, *Journal of the Taiwan Institute of Chemical Engineers* 124, 307 **(2021)**.